The Journal of Experimental Biology 208, 1817-1833
Published by The Company of Biologists 2005
doi:10.1242/jeb.01579

A 3-D kinematic analysis of gliding in a flying snake, *Chrysopelea paradisi*

John J. Socha[1,*], Tony O'Dempsey[2] and Michael LaBarbera[1]

[1]*Department of Organismal Biology and Anatomy, University of Chicago, Chicago, IL, 60637, USA, USA* and [2]*Leica Geosystems (Singapore) Pte Ltd, 25 International Business Park, #02-55/56 German Centre, Singapore 609916*

*Author for correspondence (e-mail: jjsocha@midway.uchicago.edu)

Accepted 9 March 2005

Summary

Flying snake species (*Chrysopelea*) locomote through the air despite a lack of appendages or any obvious external morphological specialization for flight. Here photogrammetric techniques were used to investigate *C. paradisi*'s aerial trajectory in three dimensions. Two videocameras arranged in stereo were used to record head, midpoint and vent landmarks on snakes that jumped from a horizontal branch at a height of 9.62 m and landed in an open field. The coordinates of these landmarks were reconstructed in three dimensions and used to analyze patterns of position, glide angle and speed concurrently with changes in body posture in 14 glide sequences from different individuals. *C. paradisi*'s trajectory was composed of a ballistic dive followed by a shallowing phase in which the path became more horizontal; for most glide trials, no equilibrium phase was observed. In the ballistic dive, the snake changed posture from generally straight to a wide 'S' shape in planview and began aerial undulation. Shortly after the ballistic dive, the snake's speed transitioned from an initial acceleration to stable or to a different rate of increase or decrease. Aerial undulation, in which high-amplitude traveling waves pass posteriorly down the body, was a prominent locomotor behavior. In mid-glide, this undulation occurred with the anterior body oriented approximately parallel with the ground and the posterior body cycling up and down in the vertical plane. The body angle of attack for the anterior body for one trial was 20–40°. Snakes traveled a horizontal distance of 10.14±2.69 m (mean ± S.D.) while reaching an airspeed of 10.0±0.9 m s^{-1}, sinking speed of 6.4±0.8 m s^{-1} and horizontal speed of 8.1±0.9 m s^{-1}. The glide path shallowed at a rate of 20±6° s^{-1} and reached a minimum glide angle of 28±10°, with a minimum recorded glide angle of 13°. *C. paradisi* are surprisingly good gliders given their unconventional locomotor style, with performance characteristics that rival or surpass more familiar gliding taxa such as flying squirrels. As in other gliders, *C. paradisi* is potentially capable of using aerial locomotion to move effectively between trees, chase aerial prey, or avoid predators.

Supplementary material available online at
http://jeb.biologists.org/cgi/content/full/208/10/1817/DC1

Key words: snake, gliding, flight, locomotion, performance, kinematics, *Chrysopelea paradisi.*

Introduction

Despite the apparent constraints of having a cylindrical, limbless body plan, arboreal colubrid snakes of the South and Southeast Asian genus *Chrysopelea* locomote through the air (Socha, 2002b). Most knowledge of their aerial movements has come from anecdotal reports, which documented that they jump from a high perch (Daly, 1899; Flower, 1899; Pendlebury, 1931; Shelford, 1906), flatten the body dorsoventrally (Shelford, 1906), parachute or glide through the air while undulating from side-to-side in a swimming-like fashion (Vaughn-Arbuckle, 1959) and land at a level lower than their takeoff. There have been no experimental studies of snake flight performance other than an estimate of aerial speed for two *C. ornata* dropped by hand from a tower (Heyer and Pongsapipatana, 1970). *Chrysopelea* species represent the only limbless vertebrate flyers (including passive and powered flight) and, thus, present interesting questions of aerodynamics, morphology and evolution of flight. In this study, we quantify and characterize the aerial behavior, kinematics and performance of one species of flying snake in semi-natural conditions.

Most previous studies of vertebrate gliders (e.g. flying squirrels) have determined aerial performance using distance between takeoff and landing locations to estimate angle of descent and speed (e.g. Jackson, 1999; Vernes, 2001; Young et al., 2002; but see McGuire, 1998 as a counter example). However, because lift production is a non-linear function of airspeed (Vogel, 1994), the descent of any gliding animal starting from rest must follow a non-linear path. Therefore

studies that focus on a 'steady phase' of gliding may not adequately characterize gliding performance. Furthermore, gliders modify body posture and wing shape to effect changes in trajectory (e.g. Jackson, 1999). How such behavioral regulation relates to changes in performance is unknown. Compared with the relatively minor bodily adjustments used by other gliders, correlations between posture and performance may be most clearly and easily identified in the large-scale body oscillations used by *Chrysopelea*.

The genus *Chrysopelea* is composed of five species (Mertens, 1968) and is likely to be a monophyletic assemblage. *Chrysopelea* are active, diurnal snakes that inhabit lowland rainforests and whose diet primarily consists of lizards and, occasionally, birds and bats (Tweedie, 1960, 1983). Beyond these broad observations of lifestyle, there have been no in-depth studies regarding how they use aerial locomotion in the wild. In general the advantages of being able to aerially locomote, even if the animal can only move downward in still air, are obvious – the ability to fall safely while gaining horizontal distance potentially broadens an animal's behavioral repertoire and ecospace (Norberg, 1985, 1990; Rayner, 1981). Both parachuters (*sensu* Oliver, 1951), which fall a greater vertical distance than travel horizontally, and gliders, which travel farther horizontally than they fall, can use aerial locomotion to cross space between trees or to move to the ground. In the descent, kinetic energy of movement comes from the conversion of potential energy due to relative height. Not only does this entail less energy usage than in crawling down the tree, across the ground and up the target tree (Caple et al., 1983; Dial, 2003; Norberg, 1981, 1983), but in flying the glider may encounter fewer predators along the way; however, both assertions are generally lacking in empirical data (Scheibe and Robins, 1998). If they do encounter a non-flying predator while perched on the tree, they can become airborne to escape. Furthermore, they can potentially chase prey that become airborne themselves, although this seems to be the least likely to actually occur in the wild.

In this study, we examine the aerial locomotor ability of *C. paradisi*, which has been hypothesized by Mertens (1970) to be the 'true glider' (i.e. glide angle less than 45° during steady gliding; Oliver, 1951) of the flying snakes. In particular, we address the following questions: is *C. paradisi*'s aerial descent simply drag-based parachuting in which the snake falls as a projectile, or does the snake generate enough lift to introduce a significant horizontal component to the trajectory? If *C. paradisi* is indeed a true glider, at what point in the trajectory does the snake reach equilibrium (Vogel, 1994)? To answer these questions, it is necessary to examine how the speed of the snake and the shape of the trajectory change through time and space, and if changes in aerial locomotor posture relate to changes in performance within the trajectory. We used video photogrammetry to obtain the 3-D coordinates of the head, midpoint and vent of individual snakes throughout their aerial trajectory in a semi-natural setting. These coordinates are used to describe the snake's aerial kinematics in detail and estimate the basic characteristics of snake flight, and represent the first full 3-D analysis of any glider's trajectory. Results from this study will serve as a framework for future studies of flying snake aerodynamics, morphology and evolution.

Materials and methods

Animals

Twenty-one *C. paradisi* (Boie) wild-caught in Singapore were observed in the course of this study. Results from 14 individuals whose trajectories met the criteria for inclusion are reported here. Snakes ranged from 3.0 to 82.7 g in mass and from 31.0 to 86.5 cm in snout–vent length (SVL). The smallest snake was a young juvenile, with an estimated age of 2–4 months (Mundkur, 1978); the largest snakes were fully developed adults. Both males and females were used. The purpose of this study was to explore the full range of performance within this species; explicit analyses of size effects on performance are reported in Socha and LaBarbera (2005).

Snakes were housed in a non-public animal room in the Reptiles Division of the Singapore Zoological Gardens, following standard approved zoo protocol. Snakes were kept in 10-gallon aquaria with copious branches and water and were fed wild-caught geckos once per week. No trials were conducted on the two days following feeding. Because the animal room was open-air, temperature (25–32°C) and relative humidity (50–70%) were similar to ambient conditions of the snakes' natural habitat. Animal care and experimental procedures were approved by the University of Chicago Animal Care and Use Protocol Committee (IACUC #70963).

Experimental setup

Snakes were launched from a specially constructed scaffolding tower in an open, grassy field in the Singapore Zoological Gardens (Fig. 1A). Snakes jumped under their own power (see Movies 1 and 2 in supplementary material) from a branch secured to the tower at a height of 9.62 m. The branch was approximately straight, tapering in diameter from 4 cm at the base to 2 cm at the tip, and protruded 1 m from the edge of the tower's platform. The branch was chosen for its sufficient roughness, as *Chrysopelea* have trouble gripping smooth or debarked branches. A blue fabric sheet was hung adjacent to the branch to shield a stand of trees in the rightmost corner of the field from the snake's field of view. The coordinate system was defined relative to the front of the tower, with the *x*-axis oriented to the side, the *y*-axis oriented to the front and the *z*-axis oriented vertically.

Two Sony DCR-TRV900 digital videocameras (NTSC standard; Tokyo, Japan) were positioned at the top of the tower, approximately 12 m above the ground. In accordance with standard photogrammetric techniques, they were placed as far apart as possible (~2 m) to maximize base:height ratio, important to the 3-D coordinate reconstruction process. Each camera was attached to a mount and secured to the side of the tower to minimize camera vibration. Vibration was not discernible in the video records; digitization of a fixed point

throughout the snake's trajectory showed only random scatter and was consistent among trials. For all recording, videocameras used effective shutter speeds between 1/1000–1/2000 s and recorded at 30 interlaced frames per second. Video sequences were synchronized *post hoc* by matching short-duration, high amplitude peaks in the audio signals. The smallest effective focal length (nominally 4.3 mm, equivalent to 41 mm in 35 mm photography) was used to obtain the largest field of view. For some trials, the cameras were placed lower on the tower (at a height of approximately 5.8 m) to record a closer view of the gliding phase of the trajectory; such trials were used to obtain greater details of the snake's postural changes in mid-glide.

A grid of evenly distributed reference points (known as control points; Fig. 1A), covering an area approximately 8×8 m, was placed within the field of view of the videocameras as a position and orientation reference. These points provided the photogrammetric basis for the 3-D determination of the snake's landmark positions. The relative positioning of the control points was determined to the nearest 0.1 mm using standard terrestrial surveying techniques. The digitizable region of the glide arena (in which the videocameras overlapped in view) was roughly pyramidal in shape, with the apex located at the cameras and the base ranging from ~2 to 14 m from the bottom of the tower.

Two Nikon SLR cameras (models F5 and F100; Tokyo, Japan) were used to capture specific aspects of posture throughout the trajectory. Two primary setups were used. The first was at the base of the tower, with the camera angled upward to record a ventral view of the snakes after takeoff. The camera was aligned such that the lens axis was roughly perpendicular to the ventral surface of the snake during that point in the trajectory. In addition to posture, these images were used to calculate wing loading. The second general position was on a scaffolding tower located ~10 m to the side of the main launch tower. These views were used to obtain lateral posture information.

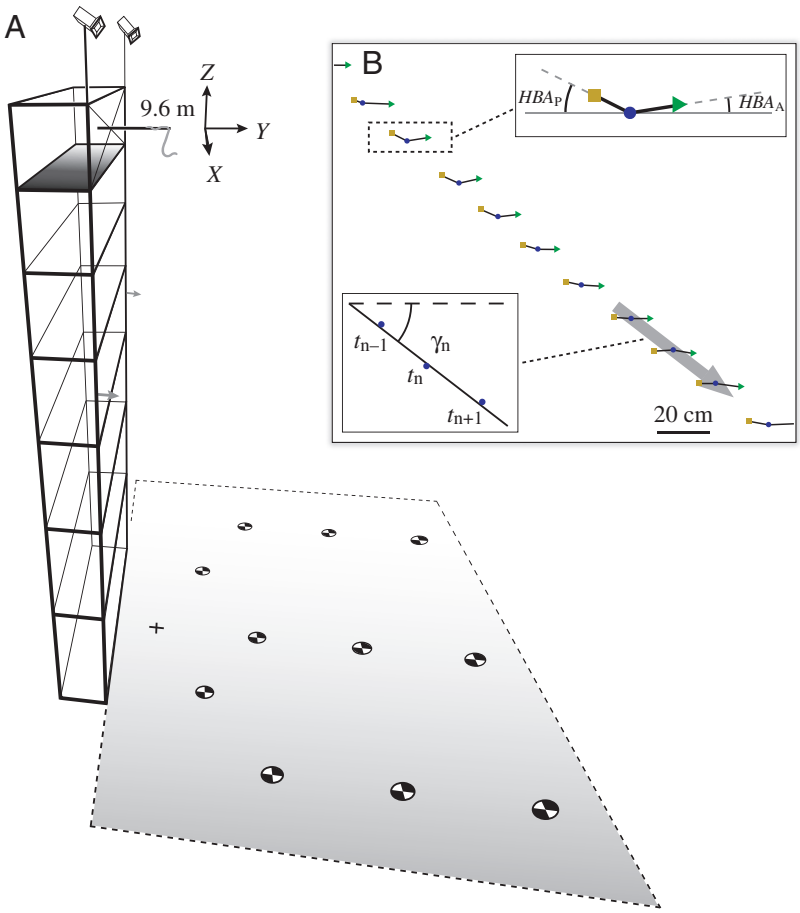

Fig. 1. Setup and trajectory variables. (A) Observational setup. Snakes were launched from a horizontal branch (height=9.62 m) at the top of a scaffolding tower in the Singapore Zoological Gardens. Two digital videocameras recorded a stereo view of the trajectories from a position approximately 2.5 m above the branch (Position 1). In a few trials, the cameras were placed lower on the tower (at a height of approximately 5.8 m; Position 2) to record a closer view of the gliding phase of the trajectory (grey arrows). Markers were placed in the field in a rough 2 m grid to serve as reference points for the 3-D coordinate reconstruction; an average of eight were used per trial. An arbitrary reference system was set up with the *Y* axis projecting forward (perpendicular to the tower face), the *X* axis to the side (parallel to the tower face) and the *Z* axis in the vertical, with the origin (+) located at the ground directly beneath the distal tip of the branch. (B) Definition of glide angle and horizontal body angle. Sequence is a side view of a trajectory at an early stage of the shallowing glide. Points represent the head/body junction (triangles), body midpoint (circles) and vent (squares) from one snake during one trajectory, sampled at 30 Hz. Temporal sequence is from upper left to lower right. Instantaneous glide angle (inset, lower left) was calculated as the angle between the principal axis of variation of three consecutive midpoint coordinates and the horizontal plane. Anterior and posterior horizontal body angles (inset, upper right corner) were calculated as the angle between a line connecting the head to the midpoint and the horizontal plane (HBA_A) and as the angle between a line connecting the midpoint to the vent and the horizontal plane (HBA_P). HBA_P values were given a negative sign convention relative to HBA_A so that equal angles indicate equivalent body postures. Scale bar, 20 cm.

Glide trial protocol

During glide trial days, snakes were kept in individual cotton reptile sacks placed in a styrofoam container in a shaded location. Ambient air temperature was recorded every half hour with a Kestrel 2000 digital anemometer/thermometer (Nielsen-Kellerman, PA) placed in the open air at eye level on the launch platform. On days with wind, we coordinated the release of the snake onto the branch with lulls in the wind and noted the wind speed immediately after the glide. A better indicator for the presence and relative magnitude of wind during a glide was the blue sheet, which waved in winds as low as 0.1 m s^{-1} and could be evaluated *a posteriori* from the video records. For most trials there was no

noticeable wind; the maximum recorded windspeed was less than 0.5 m s^{-1}.

To create visible landmarks, the snakes were marked on the dorsal surface at the head body junction (hereafter, 'head'), body midpoint and vent with a one-centimeter band of non-toxic white paint (Wite-Out, Waterman-BIC, Milford, CT, USA). For the young juvenile snake, care was taken to use a minimum amount of paint to prevent a significant increase in mass of the snake.

In preparation to launch, snakes were removed from the reptile sack and placed by hand onto the proximal end of the branch, with the snake's head facing away from the tower. The snake usually moved toward the end of the branch and either stopped or began takeoff immediately. In trials in which the snake hesitated, it was gently prodded on the posterior body and/or tail to try to elicit an escape response. Snakes that didn't respond within 10 min were removed from the branch.

Upon landing of the snake, two volunteers recaptured the snake and marked the location where the tail contacted the ground. The *X*, *Y* position of landing was measured with a tape measure, using a spot on the ground directly below the tip of the branch as the origin (Fig. 1A). Because the volunteer marking the landing location was running and the snake usually kept moving after hitting the ground, there was a fair degree of placement error, sometimes as high as 50 cm. This error was minimized through verification or adjustment from the video records. Landing location data were used to corroborate the reconstructed 3-D trajectory coordinates.

Individual snakes were sampled multiple times per day, with at least 15 min of recovery between trials. Observational days were usually followed by a day of rest. A total of 237 trials were recorded, averaging 11 per snake. Here we analyze a subset of these trials in detail to illustrate specific aspects of kinematics and behavior and to characterize gliding in *C. paradisi*. Fourteen trajectories, each representing a different snake, were chosen using the following criteria. (1) The size of the snakes spanned the range of the sample. (2) The quality of video was high (in regard to lighting, ease of identifying landmarks and percentage time that the snake's landmarks were in view). (3) Because this study is concerned with the limits of aerial ability, the 'best' glide for each snake was used, where 'best' was evaluated as greatest horizontal distance traveled. When the farthest trajectory for a particular snake was not suitable for analysis (according to criterion 2), the next farthest trajectory was used.

3-D coordinate reconstruction

The video records of the glide trials were transferred at highest quality to a Macintosh G4 computer *via* Firewire (IEEE 1394) using Adobe Premiere (version 6.0) software, with a raw image size of 720×480 pixels. Sequences were deinterlaced to yield 60 video fields per second and exported as a series of 'pict' image files, which were converted to maximum-quality 'jpg' files using Adobe Photoshop. Synchronization was verified (and/or adjusted) by comparing movements of the snake in both sets of images. The jpgs were imported into ERDAS Imagine software (version 8.4; Leica Geosystems GIS and Mapping, LLC, Atlanta, USA) and converted to ERDAS's proprietary 'img' format. This image conversion process had no effect on image quality. The head, midpoint and vent landmark points of the snake were digitized in each image pair at a sampling frequency of 30 Hz. (Although 60 Hz data were available, an initial test determined that the additional temporal resolution was unnecessary for interpreting spatial, glide angle and velocity patterns.)

ERDAS Imagine w/Orthobase (version 8.4) software was used to reconstruct spatial coordinates in three dimensions. Orthobase uses the direct linear transformation (DLT) method (Abdel-Aziz and Karara, 1971) to transform coordinates between a 2-D image plane through the camera and a 3-D object space. DLT is a commonly used method to reconstruct 3-D coordinates in studies using non-metric cameras (e.g. Ambrosio et al., 2001; de Groot, 2004; Douglas et al., 2004; Gruen, 1997; Meintjes et al., 2002). Assuming collinearity, the image point, focal point of the camera and object point are calculated to lie on a straight line (one per point per image) based on the following DLT equations:

$$x + \partial x + \Delta x = \frac{L_1X + L_2X + L_3X + L_4}{L_9X + L_{10}Y + L_{11}Z + 1}$$

$$y + \partial y + \Delta y = \frac{L_1Y + L_2Y + L_3Y + L_4}{L_9X + L_{10}Y + L_{11}Z + 1}, \quad (1)$$

where *X*, *Y* and *Z* are the spatial coordinates of a point in 3-D object space, *x* and *y* are the two coordinates of that point mapped onto the 2-D image space, δx and δy are nonlinear systematic errors, Δx and Δi are random errors, and the coefficients L_i are the 11 DLT parameters. In this study, each stereo video image pair contained complementary views of the control points on the ground and the snake in the air. Thus each control point, for which both the image space and object space coordinates were known, generated four equations. Using data from a minimum of six control points and the exterior orientation (the spatial and angular position of the cameras), the DLT parameters were calculated; these descriptors constitute the DLT model. After the model was determined, the digitized *x*, *y* coordinates of the snake's head, midpoint and vent landmarks in each image pair were used used to calculate their respective *X*, *Y* and *Z* coordinates. See (Chen et al., 1994; Gruen, 1997; Maas, 1997; Yuan and Ryd, 2000) for further details of DLT methodology.

Quality of data

The combination of the large size of the glide arena, the low base/height ratio of the cameras and the small amount of variation in the vertical axis of the reference points constrained the quality of data produced in this study. Given the small variance in vertical axis of the reference points, photogrammetric reconstruction was made possible by measuring the position of the cameras (within a few centimeters) and restricting their adjustment in Orthobase such

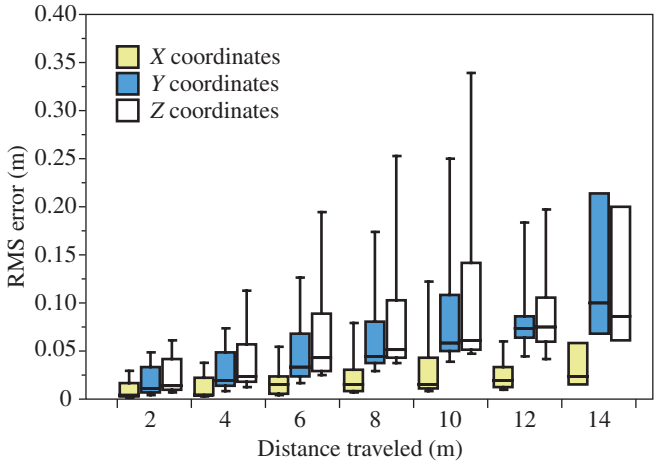

Fig. 2. Pooled RMS coordinate errors for midpoint coordinates. Each box represents the standard quartiles of the pooled distribution of all 14 trajectories at each spatial interval. Distance traveled represents the straight-line distance from the respective trajectory coordinate to the takeoff location. Error bars represent 10th and 90th percentiles, respectively.

that they were relatively fixed in space (using a standard deviation of 5 cm). RMS coordinate error (which includes digitization error, equipment error and 3-D reconstruction error) was calculated for each landmark using Orthobase. In general, error increased throughout the trajectory (Fig. 2), a standard feature of stereophotogrammetric systems (e.g. Yuan and Ryd, 2000); as the snake moved away from the cameras, it became smaller in the field of view and the relative parallax between images decreased, increasing the error. For the midpoint, the mean RMS error ranged from 1–4 cm, 2–14 cm and 3–13 cm in the *X*, *Y* and *Z* axes, respectively (Fig. 2). At any point, the error in the *X*-axis coordinates was 2–4 times smaller than that in other two axes. The midpoint error was slightly lower than that of the head and vent, likely because these points were more difficult to identify. Landmarks were also generally more difficult to digitize on small snakes because their dorsal surface areas were smaller. Color contrast was a problem in the latter portion of the trajectory, with the green and black snake obscured against the green grass background. In future studies, increased spatial resolution can be accomplished by increasing the contrast between the snake and the background, by using more cameras, by placing the cameras closer to the area of interest and farther apart from each other, and by introducing more vertical variation amongst the control points.

Trajectory variables

The following variables were used to characterize the gliding performance of snakes throughout their aerial trajectory. In general, a glider's trajectory begins when its entire body becomes airborne. In this study we ignored the snake's initial upward motion in the air (due to takeoff) and defined trajectory as starting from the downward motion of the snake. In practice, the trajectory was taken as the path of the snake from the video field preceding the first downward movement of the snake's midpoint coordinate (at the apex of the arc resulting from takeoff) to the video field in which the midpoint contacted the ground. Although the takeoff was ignored, in all the trials analyzed here the snake launched itself from the branch using a vertically looped takeoff, usually of the 'J-loop' variety (Socha, 2002b).

Glide angle (γ)

Glide angle is the angle between a tangent to the local trajectory of the snake and the horizontal plane (Fig. 1B). In equilibrium gliding, it is a simple function of the lift-to-drag ratio (see below) and therefore a primary descriptor of performance for a glider. The smaller the glide angle, the more horizontal the trajectory and the farther the snake can potentially travel. Glide angles reported here are instantaneous glide angles, (γ_n), defined as the angle between a best-fit line through the coordinates and the horizontal plane, calculated using sets of three temporally consecutive coordinates. Because the coordinates are 3-D, the principal axis of variation (analogous to a least-squares line in 2-D; see Socha, 2002a) was used as the best-fit line. Glide angles were calculated for all three landmarks, but only those calculated from the midpoint coordinates are reported here; midpoint coordinates were the most abundant (in terms of visibility) and gave glide angles with the least variation, which provides evidence that the midpoint was the landmark closest to the snake's true center of gravity in any postural configuration. For comparison, glide angles for a theoretical projectile launched at the same height and initial velocity as the snakes were also calculated using standard equations of motion. Because a theoretical projectile encounters no drag or lift, it offers the most conservative estimate of change in glide angle due to aerodynamic forces on the snake.

Glide ratio

The ratio of horizontal distance traveled to height lost is also commonly used to describe a glider's performance. The larger the glide ratio, the farther the glider can travel in a given vertical drop. In equilibrium, glide ratio is equivalent to the ratio of lift-to-drag and is equal to the cotangent of the glide angle (Vogel, 1994):

$$\frac{L}{D} = \cot\gamma\,. \qquad (2)$$

We used the minimum glide angle to calculate glide ratio for a trajectory.

Ballistic dive angle (γ_{BD})

At the start of a trajectory, a glider has low airspeed. Because lift production is approximately proportional to the square of the speed, the magnitude of lift is initially small. The phase in which the glider falls like a projectile is the ballistic dive. A glider dropped from rest (with a positive angle of attack) would start with a glide angle near 90°, and this angle would decrease as speed increased. Because the snake's jumping takeoff

imparted a horizontal velocity component to the initial trajectory, glide angle was initially near zero, increased to a maximum and decreased thereafter. We defined the ballistic dive angle as the maximum glide angle during this phase. Because the shape of the trajectory is a smooth spatial function, there was no spatially discrete end to the ballistic dive. Therefore, the end of the ballistic dive phase was defined as the point where the glide angle began to decline.

Trajectory shallowing rate

As a glider's speed increases, increasing lift production causes the trajectory to shallow. The trajectory shallowing rate is defined as the rate at which the glide angle changes during the shallowing phase. It was calculated using a least-squares regression of the glide angle as a function of time. Only the linear portion of the curve (chosen by eye) were used in the regression.

Speed and acceleration

Airspeed is the speed of the snake along its trajectory, calculated using the distance between the 3-D coordinates. Prior to calculating airspeed, the digitized coordinates were smoothed using QuickSAND software (Walker, 1997) with a Lanczos five-point moving regression, which takes a weighted average of the two smoothed values immediately prior to and following the point of interest (Walker, 1998). This algorithm was chosen because it most accurately reproduced the original data. Sinking speed and horizontal speed were calculated in the same manner as airspeed using the vertical and horizontal components of the coordinate data, respectively. Acceleration in the initial trajectory was estimated using least-squares regression of speed *vs* time in the region of linear increase (identified by eye).

Heading angle

Heading angle is the direction of travel of the snake along its trajectory as projected onto the horizontal plane, using three temporally successive (*X*, *Y*) positions of a given body landmark to define a local flight path. The angle between a least-squares fit line calculated using these three points and the Y-axis was the instantaneous heading angle. Separate heading series were calculated for the head, midpoint and vent, all of which oscillated about the heading of the snake's center of gravity. Because the center of gravity was not digitized, an average heading of the snake was estimated based on the three landmarks. The average heading data were used to determine the relative positioning of the three landmarks and can be used to identify turns, which are not examined here.

Postural variables

The following variables were used to quantify the snake's aerial locomotor behavior, defined as postural changes in the trajectory (Emerson and Koehl, 1990; McCay, 2001). It should be noted that performance and behavior variables may be conflated, as it is difficult to assess *a priori* which features are actively under the control of the snake, which are a consequence of aerodynamic forces, or both.

Excursion (vertical, fore–aft, lateral)

The most straightforward metric of posture is the relative spatial positioning of the landmarks. We defined vertical, fore–aft and lateral excursion as the perpendicular distance of the head or vent to the midpoint (relative to the snake's direction of travel, calculated using instantaneous heading angle).

*Horizontal body angle (*HBA*)*

The horizontal body angle is the angle between the body axis and the horizontal plane (Fig. 1B). It was calculated as an indicator of the degree of incline of the snake's body relative to the ground. Horizontal body angles were calculated for both the anterior (head to midpoint, HBA_A) and posterior (midpoint to vent, HBA_P) segments.

Body angle of attack (α_B)

In aerodynamics, angle of attack is the angle between the chord line of the airfoil (the line that connects the leading and trailing edges) and the direction of oncoming airflow. Angle of attack is an important aerodynamic parameter – in general, as angle of attack increases, lift and drag increase until stall occurs (Bertin, 2001). Because the orientation of local camber was not recoverable based on the coordinate data alone, a body angle of attack was used as a proxy for true angle of attack. We defined body angle of attack as the angle between a segment's body axis and the local trajectory, calculated by summing the instantaneous glide angle and the horizontal body angle:

$$\alpha_{B,n} = \gamma_n + HBA_n \, . \quad (3)$$

Body angle of attack was calculated separately for both the anterior and posterior body segments.

Wing loading

Wing loading is the weight of the flyer divided by the projected area of the wings. For gliders, the higher the wing loading, the higher the speed needed to maintain an equilibrium glide (Vogel, 1994). Wing loading also affects maneuverability – all else being equal, gliders with higher wing loading are generally less maneuverable (Emerson and Koehl, 1990; Norberg et al., 2000). Because it is not known which parts of the snake act as a functional 'wing', the projected area of the entire snake (including the tail) was used to calculate wing loading (*WL*):

$$WL = \frac{W}{S} \, , \quad (4)$$

where *S* is area and *W* is the weight of the snake. Projected area was measured in NIH Image (version 1.62, National Institutes of Health, Bethesda, Maryland, USA) using photographs of the ventral surface of the snake (e.g. Fig. 3). Images were internally calibrated using the known snout–vent length of the snake. The coordinates of the midline of the snake

were digitized in NIH Image, smoothed in QuickSAND and interpolated to 1000 points; the total distance between these points was used as the reference length. Any non-orthogonality of the snake in relation to the camera was not systematically taken into account. Error due to non-orthogonality is a function of the cosine of the angle of rotation away from planar, resulting in an underestimate of wing area. Therefore wing loading values presented here err in the direction of overestimation. For example, if a snake was rotated 25° from orthogonal when photographed, its calculated wing loading would be overestimated by 9%.

Undulation frequency

The snake's swimming-like motion is a form of aerial undulation, in which traveling waves pass posteriorly down the body. Undulation frequency, the frequency of these waves, is defined as the frequency of side-to-side movement of the head or vent about the axis determined by the direction of travel. It was calculated as the inverse of the undulation period, the time interval between successive peaks of head lateral excursion.

Undulation wave height

Undulation wave height is the maximum height of the traveling waves, a measure of the total width of the snake in the aerial 'S' posture (Fig. 3). Because it was not possible to measure this width directly from the video records, the maximum lateral separation between the midpoint and the vent was used as a proxy for wave height. It is a proxy because the maximum lateral separation between the midpoint and vent is 50% SVL (by definition) and it is theoretically possible for the wave height to be greater than 50%. Undulation wave height was calculated as one-half the vertical distance between peaks of the head and vent lateral excursion. The maxiumum side-to-side speeds of the head and vent were estimated by multiplying the undulation wave height by the undulation frequency.

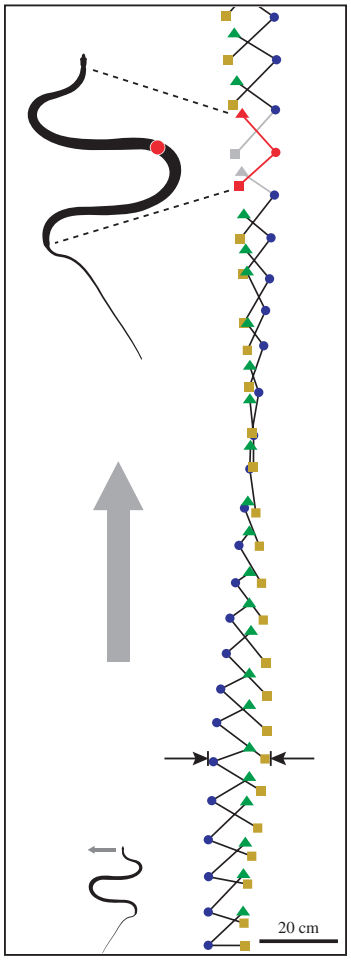

Fig. 3. Overhead view of snake's landmarks during aerial undulation. Points represent the head/body junction (triangles), body midpoint (circles) and vent (squares) from one snake during one trajectory, sampled at 60 Hz. Temporal sequence is from bottom to top. As the snake moves forward along the trajectory, traveling waves move posteriorly down the snake, producing a side-to-side undulatory pattern in which the head and vent move out of phase with the midpoint. At the beginning of the sequence shown, the head is moving to the left relative to the midpoint. The frequency of undulation and maximum wave height (approximately the distance between the paired black arrows) were 1.3 Hz and 24% SVL, respectively, with an average airspeed of 6 m s^{-1}. Scale bar, 20 cm.

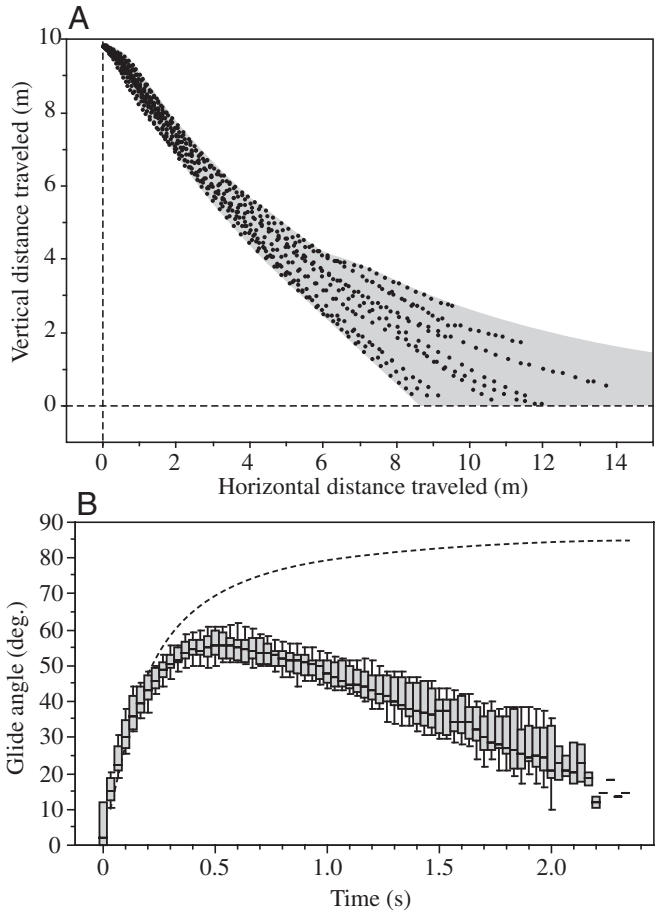

Fig. 4. Trajectory and glide angle summary plots. Fourteen trajectories, each from a different snake, are shown. (A) Side view of trajectories. Data are unsmoothed 3-D coordinates sampled at 30 Hz, rotated about the average heading angle prior to plotting. The gray shading represents the range of trajectory space of the trials. Trajectories are similar in the first 5 m of vertical drop and then diverge, with the snakes shallowing at different rates. (B) Pooled glide angle through time. Each box represents the standard quartiles of the pooled distribution of all 14 trajectories at each time interval. Error bars represent 10th and 90th percentiles, respectively. The dotted line represents the glide angle of a theoretical projectile launched with an initial horizontal velocity of 1.7 m s^{-1}. For the snakes, glide angle began near zero, increased rapidly and deviated from the theoretical projectile early, approximately where aerial undulation began.

Table 1. *Summary data for* C. paradisi *aerial locomotion*

	Mean ± S.D.	Min.	Max.	*N*
Snakes				
Mass (g)	40.5±23.1	3.0	82.7	14
Snout–vent length (cm)	68.6±15.7	31.0	86.5	14
Tail length (cm)	23.2±6.2	9.6	29.4	14
Wing loading (N m^{-2})	29±9	12	46	11
Trajectory performance				
Trajectory time analyzed (s)	1.95±0.22	1.53	2.37	14
Vertical distance analyzed (m)	8.61±1.05	7.04	9.86	14
Horizontal distance, total (m)	10.14±2.69	6.28	14.29	14
Ballistic dive angle (degrees)	57±3	52	62	14
Ballistic dive time (s)	0.72±0.18	0.40	1.03	13
Ballistic dive depth (m)	2.32±1.12	0.95	5.21	13
Shallowing rate (degrees s^{-1})	20±6	11	36	14
Glide angle, min (degrees)	28±10	13	46	14
Glide ratio, max	2.2±1.1	1.0	4.2	14
Airspeed at takeoff (m s^{-1})	1.7±0.6	0.8	2.8	14
Forward acceleration, initial (m s^{-2})	7±1	5	10	14
Sinking acceleration, initial (m s^{-2})	6±2	3	11	14
Horizontal acceleration, initial (m s^{-2})	4±1	3	6	14
Time at airspeed transition (s)	1.11±0.31	0.63	1.67	12
Time at sinking speed transition (s)	0.93±0.22	0.53	1.30	13
Time at horizontal speed transition (s)	1.58±0.15	1.37	1.90	9
Airspeed at transition (m s^{-1})	8.9±1.4	6.1	11.0	12
Sinking speed at transition (m s^{-1})	6.1±0.7	4.5	7.2	13
Horizontal speed at transition (m s^{-1})	8.3±1.1	6.3	9.7	9
Airspeed, max (m s^{-1})	10.0±0.9	8.1	11.0	13
Sinking speed, max (m s^{-1})	6.4±0.8	4.9	7.3	13
Horizontal speed, max (m s^{-1})	8.1±0.9	6.4	9.3	13
Behavior				
Undulation period (s)	0.77±0.14	0.50	1.00	13
Undulation frequency (Hz)	1.4±0.3	1.0	2.0	13
Undulation wavelength (m)	0.20±0.07	0.18	0.25	5
Undulation wave speed (m s^{-1})	0.24±0.03	0.22	0.26	3
Undulation wave height, head (cm)	0.13±0.04	0.05	0.19	13
Undulation wave height, vent (cm)	0.23±0.07	0.09	0.32	12
Undulation wave height, head (% SVL)	20±3	15	25	13
Undulation wave height, vent (% SVL)	34±5	24	43	12

Undulation wavelength and wave speed

The wavelength of the snake's traveling waves was measured in NIH Image using the same ventral-view photographs used to calculate wing loading. Wave speed was calculated by multiplying the wavelength by the undulation frequency.

Results

Trajectory

Based on glide angle, most trajectories were composed of two phases – a ballistic dive phase and a shallowing glide phase, with no equilibrium component (Fig. 4). In all trials, the ballistic dive began with a horizontal component, a consequence of the snake's takeoff velocity. The path quickly became steeper, with glide angle increasing from zero to 50° and the height dropping about 0.2 m in 0.3 s. This short portion of the ballistic dive followed the path of a theoretical projectile (dotted line in Fig. 4B). Thereafter, the trajectory deviated radically from a ballistic model, with glide angle reaching a peak of 57±3° (mean ± S.D.; Table 1). The shallowing glide began at a time of 0.72±0.18 s and a height lost of 2.32±1.12 m. In this phase, glide angle decreased at a rate of 20±6° s^{-1}. In most trials, glide angle continued to decrease throughout the entire sequence, implying that equilibrium was either not achieved or occurred after the snake exited the cameras' fields of view.

Airspeed, sinking speed and horizontal speed changed in characteristic fashion. All initially increased in the first portion of the trajectory as the snake accelerated downward (Fig. 5). After this initial acceleration, the speeds transitioned to stable or to a different rate of increase or decrease. On average (see

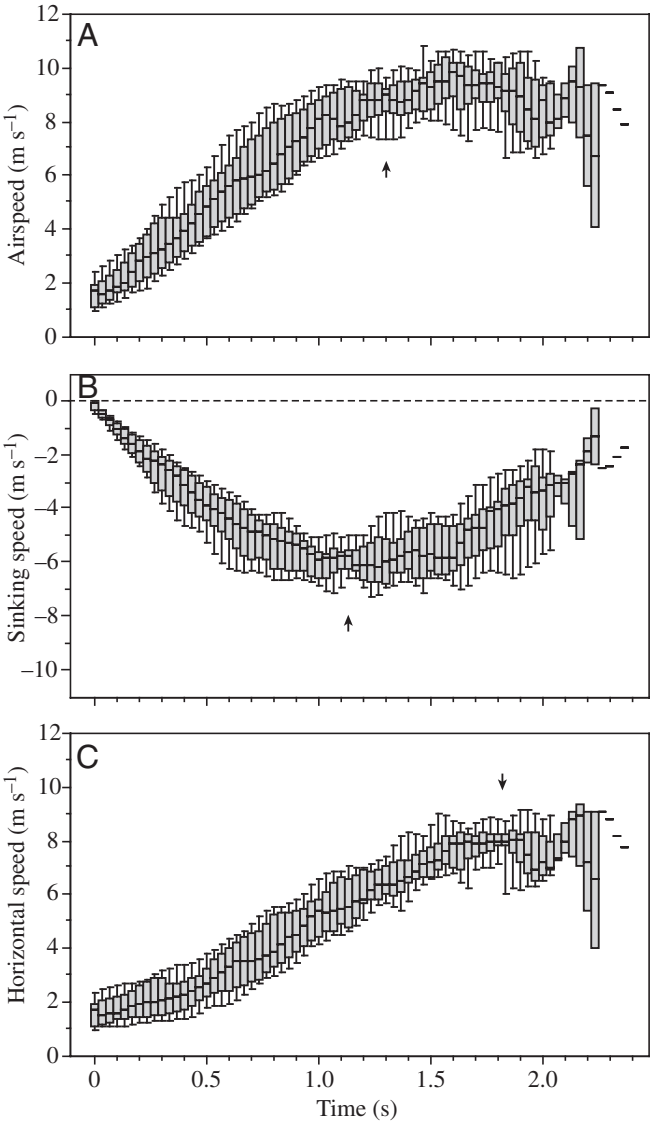

Fig. 5. Summary plots of airspeed (A), sinking speed (B) and horizontal speed (C) *vs* time. Each box represents the standard quartiles of the pooled distribution of all 14 trajectories at each time interval. Error bars represent 10th and 90th percentiles, respectively. All speeds increased early in the trajectory. Airspeed and sinking speed leveled off after about 1 s. The horizontal speed increased throughout. Note the temporary decrease in variance near the transition points (indicating the end of the initial acceleration) in each speed plot (arrows).

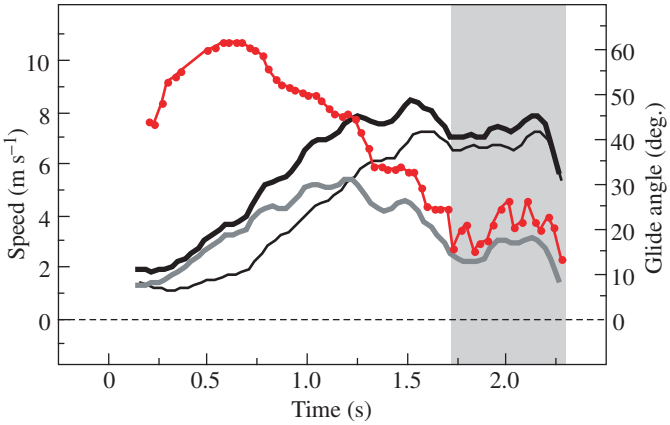

Fig. 6. Speed and glide angle *vs* time for one trajectory with possible equilibrium component. At a time late in the trajectory (gray shading), airspeed (thick black line), sinking speed (thick gray line), horizontal speed (thin black line) and glide angle (red line) all exhibit generally constant values. The cause of the oscillations in glide angle is unknown – they may be the result of the midpoint of the snake not coinciding with the effective center of mass, or they may be due to an increase in coordinate error as the snake moves away from the cameras. Mass=11 g, SVL=47 cm.

Table 1), the airspeed at the beginning of the trajectory was 1.7±0.6 m s^{-1} and increased at a rate of 7±1 m s^{-2}. At 1.11±0.31 s and 4.13±0.51 m height lost, the airspeed transitioned to level at a speed of 8.9±1.4 m s^{-1} or tapered off. This shift in airspeed is defined as the airspeed transition point. The sinking speed started from zero and increased at a rate of 6±2 m s^{-2} (which is lower than 9.8 m s^{-2}, the acceleration due to gravity). At a slightly earlier time than the airspeed (0.93±0.22 s and 3.79±0.47 m height lost), the sinking speed transitioned to level at a speed of 6.1±0.7 m s^{-1} or began decreasing. The horizontal speed initially increased at a rate of 4±1 m s^{-2} and transitioned at a later point in the trajectory (1.58±0.15 s and 5.6±0.60 m height lost). Just after the transition points for each speed type, the variance in the pooled speed data temporarily decreased (Fig. 5).

In most trials, the three speeds were never constant at the same time, which indicates that force equilibrium was not achieved. One trial was a possible exception, with a 0.4 s span near the end of the sequence where both glide angle and speed may have been constant (Fig. 6). This possible equilibrium glide occurred after a shallowing glide in which the snake dropped 4.3 m in vertical height in about 1 s. In two other trials, shallowing rate decreased near the end of the sequence, suggesting that these snakes were approaching a steady glide angle. In these three trials that came closest to equilibrium, the snakes were relatively small, with masses of 3–27 g.

Postural changes

Snakes used two behaviors: a body-organizing behavior early in the trajectory in which the snake formed a characteristic ‘S’ posture (‘S-formation’; Fig. 7A) and a high-amplitude form of undulation (‘aerial undulation’) thereafter. The snake began S-formation in an approximately straight posture with the three landmarks generally aligned along the fore–aft axis (Fig. 8). The snake was initially oriented in a ‘nose-up’ position, with the head higher than the midpoint and the midpoint higher than the vent. As the snake fell through the ballistic dive, an initial traveling wave formed anteriorly approximately 1/8 SVL from the head (Fig. 7A). As the wave began moving caudally, the head and vent were pulled inward toward the midpoint in the fore–aft direction, forming a wide

'S' shape in overhead view, and the body pitched forward into a 'nose-down' position. This phase lasted about 0.7 s.

The end of the S-formation graded into aerial undulation with the anterior segment of the snake beginning to move from side-to-side. As the initial traveling wave passed posteriorly down the body, the posterior segment began undulating about 0.2 s later. In full-body aerial undulation, the vent moved in phase with the head (Fig. 9C). Snakes undulated at an average frequency of 1.4±0.3 Hz, with posteriorly directed waves traveling at an average speed of 0.24±0.03 m s^{-1} and with an average wavelength of 0.20±0.07 m. The head and vent moved side-to-side with average maximum speeds of 0.18±0.05 and 0.30±0.07 m s^{-1} and average wave heights of 20±3 and 34±5% SVL, respectively.

Aerial undulation was not simple sinusoidal motion in a single plane. The undulation was complex, with the head and vent moving both fore and aft in the horizontal plane, and up and down in the vertical plane (Figs 8–10). The fore–aft excursion of the head was relatively small and the head never crossed behind the midpoint. The fore–aft and vertical excursions of the vent were larger than those of the head – in most undulatory cycles, the vent dropped below the level of the midpoint and moved forward, sometimes crossing in front of the midpoint. These postural changes were similar from cycle to cycle.

The horizontal body angle, which was determined by the relative vertical positioning of the landmarks, varied throughout the undulatory phase. The horizontal body angle of the anterior segment was much less variable than that of the posterior segment, which swung downward in every cycle. In one trial in which the cameras were positioned closer to the end of the trajectory, the anterior horizontal body angle remained at approximately 0° (Fig. 11A), indicating that the anterior segment of the snake was undulating in the horizontal plane. Correspondingly, the body angle of attack for the anterior segment was about 35° (Fig. 11B), but declined near the end of the sequence as the glide angle decreased. The posterior body angle of attack was similar to that of the anterior for part of the cycle, but when the posterior segment dropped below the anterior, the angle increased to as much as 110°. Thus, the coordinate data show that different parts of the body experienced different orientations to the oncoming airflow and that these orientations changed through time. There is no 'characteristic' body orientation for the snake as a whole.

The lateral view photographs provide further evidence of body orientation throughout the trajectory (Fig. 7B–D). Although qualitative in nature, these data help fill in the gaps in the coordinate data, which only provide positional information on three points on the body and do not directly indicate how each local body segment was oriented to the oncoming airflow. The images show that the snake's head and first few centimeters of the body were consistently angled downward with respect to the horizon, regardless of how the rest of the body was configured. The images also confirm that the horizontal body angle is a reasonable proxy for body orientation for the anterior half of the snake. However, it is a misleading metric for the posterior half of the body, which displays much more dramatic displacements in the vertical axis.

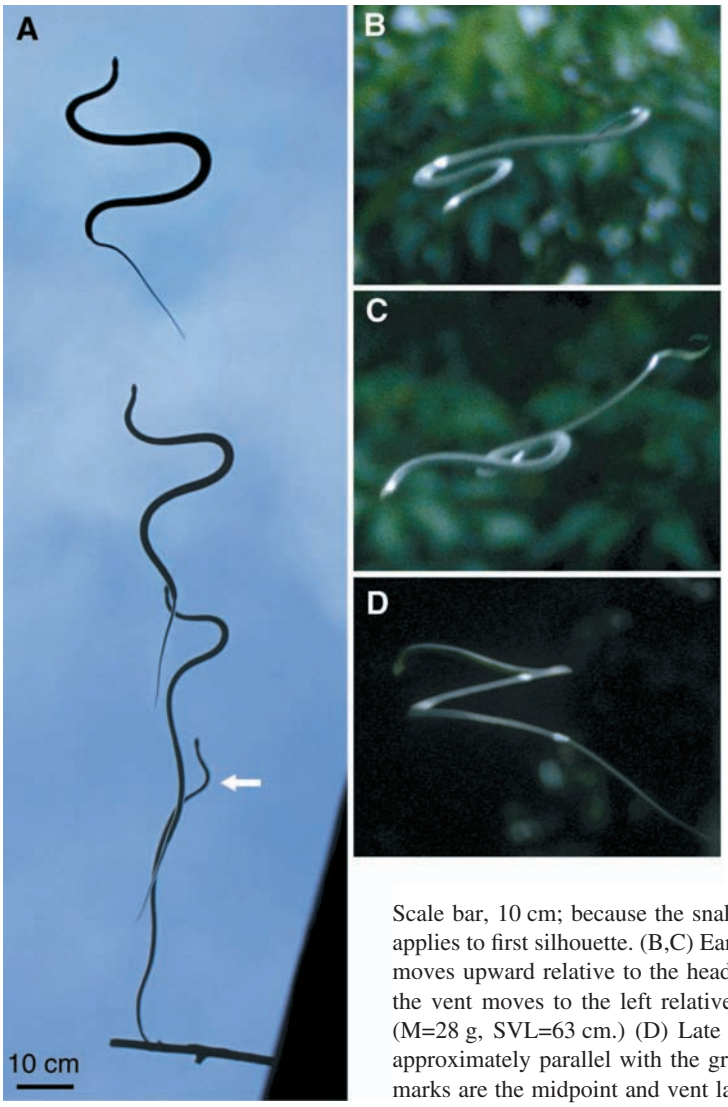

Fig. 7. Photographs of postural changes during aerial trajectory. (A) Ballistic dive, ventral view. Silhouettes composited from four consecutive photographs (200 ms intervals) of a snake (M=36 g, SVL=69 cm) at the beginning of the trajectory. Temporal sequence is from bottom to top. The white arrow shows the location of the first traveling waving formed by the snake; in successive silhouettes this wave can be seen moving posteriorly down the snake. The snake's side-to-side width increases and head-to-tail length decreases as the 'S' is formed. Scale bar, 10 cm; because the snake moved closer to the camera during the sequence, scale bar only applies to first silhouette. (B,C) Early shallowing glide phase, lateral view. In the vertical axis, the vent moves upward relative to the head and midpoint; in the lateral axis, the head moves to the right and the vent moves to the left relative to the snake's fore–aft axis. Interval between frames is 250 ms. (M=28 g, SVL=63 cm.) (D) Late shallowing glide phase, posterolateral view. The anterior body is approximately parallel with the ground and the posterior body is angled downward. The white paint marks are the midpoint and vent landmarks. (M=68 g, SVL=82 cm.)

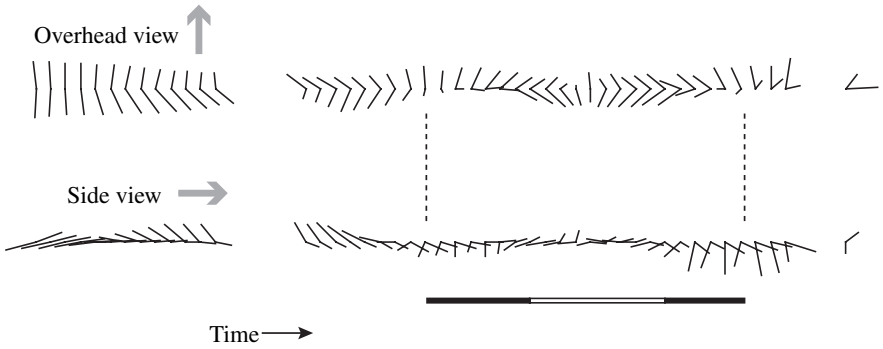

Fig. 8. Overhead and side views of postural changes through time in one trajectory. Lines represent the connections between the head, midpoint and vent, as in Figs 1 and 3. Postures are aligned by the midpoint, with the gray arrows representing the snake's forward direction of travel along the trajectory; temporal sequence is from left to right. The two gaps represent missing data. One full undulatory cycle is represented between the two dotted lines. In every cycle, the posterior segment swung lower than the anterior segment and sometimes passed in front of the midpoint. This part of the cycle (black bars) accounted for approximately half the cycle. (M=27 g, SVL=63 cm.)

For example, Fig. 7D shows a case in which the vent is below the midpoint. Here the horizontal body angle for the posterior segment (approximately 90°) would seem to indicate a perpendicular orientation relative to the horizon. However, the photograph shows that the body in between the midpoint and vent consists of two mostly-straight body segments angled laterally downward and connected by a curved segment. In each segment, the ventral surface faces downward, not at a 90° angle to the horizon.

Discussion

Given their cylindrical body plan, *C. paradisi* are surprisingly good gliders. As has been indirectly observed in other gliders (e.g. McGuire, 1998; Scholey, 1986; Vernes, 2001), *C. paradisi*'s trajectory starts with a ballistic dive and is followed by a shallowing phase in which the glide angle decreases and the sinking speed levels off or declines. During the initial portion of the trajectory, the relatively straight snake forms an 'S' shape while pitching downward and accelerating through a steep glide angle. The trajectory starts to shallow at about the same time as aerial undulation begins. The aerial undulation is non-planar, with the snake's anterior body oriented approximately parallel to the ground and the posterior body cycling between being co-planar with the anterior and swinging through a perpendicular position. Considering that glide equilibrium was not observed, the performance of *C. paradisi* described here is a conservative estimate of its ability.

Glide speed

The speed patterns provide indirect evidence of the snake's

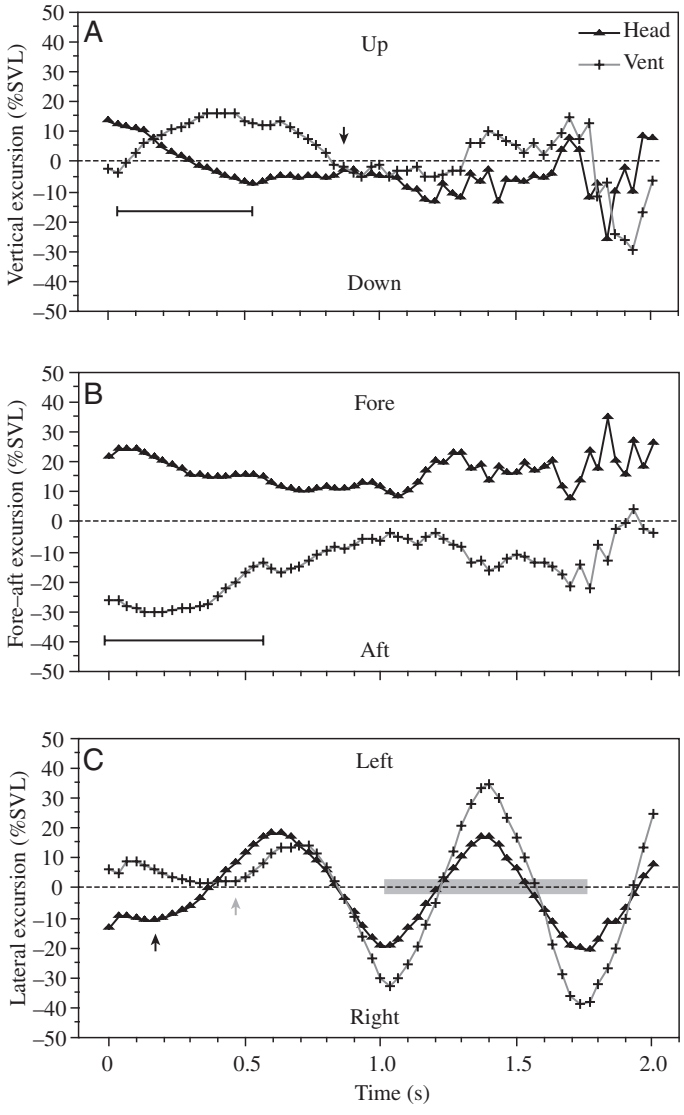

Fig. 9. Vertical, fore–aft and lateral excursion *vs* time through one trajectory. Excursion is the perpendicular distance, standardized by SVL, of the head (triangles) or vent (crosses) relative to the midpoint. (A) Vertical excursion. The head is initially higher than the other landmarks. The snake then pitches forward (indicated by bar) such that the tail is higher than the midpoint, which is higher than the head. At the arrow, the vent is brought down to the level of the head and midpoint and rises up and down thereafter. The head stays at a relatively constant level. (B) Fore–aft excursion. The head and vent are brought towards the midpoint in the S-formation phase (bar). The head shows little movement thereafter. The vent moves in slightly cyclic fashion fore and aft. For both fore–aft and vertical excursion, the error increases substantially in the last 0.4 s of the trajectory. C. Lateral excursion. Head and vent undulatory movements are clearly shown. The head undulation (first arrow) begins before the vent undulation (second arrow). In fully developed undulation, the head and vent are in phase, with the head excursion smaller than the vent excursion. The gray bar represents one full undulatory cycle. (M=36 g, SVL=69 cm.)

aerodynamic characteristics. Not surprisingly, the airspeed increased as the snake initially fell. In most trials, there was a transition point where this initial acceleration decreased abruptly, indicating a marked decrease in net force on the snake. Although this shift occurred just after aerial undulation became fully developed on average, there is no clear pattern within individual trials that relates kinematics to the timing of this transition. Young et al. (2002) noticed a similar transition in speed in parachuting geckos (*Ptychozoon kuhli*). After the transition point, airspeed became constant in some trials and increased at a lower rate in other trials, a difference that may be size dependent. Sinking speed also shows a transition point almost concurrent with the airspeed transition. Unlike airspeed, sinking speed decreased in some trials, indicating that the upward force on the snake was increasing. The temporary decrease in variance just after the speed transition points may indicate a physical constraint in which snakes are confined to pass through a particular speed.

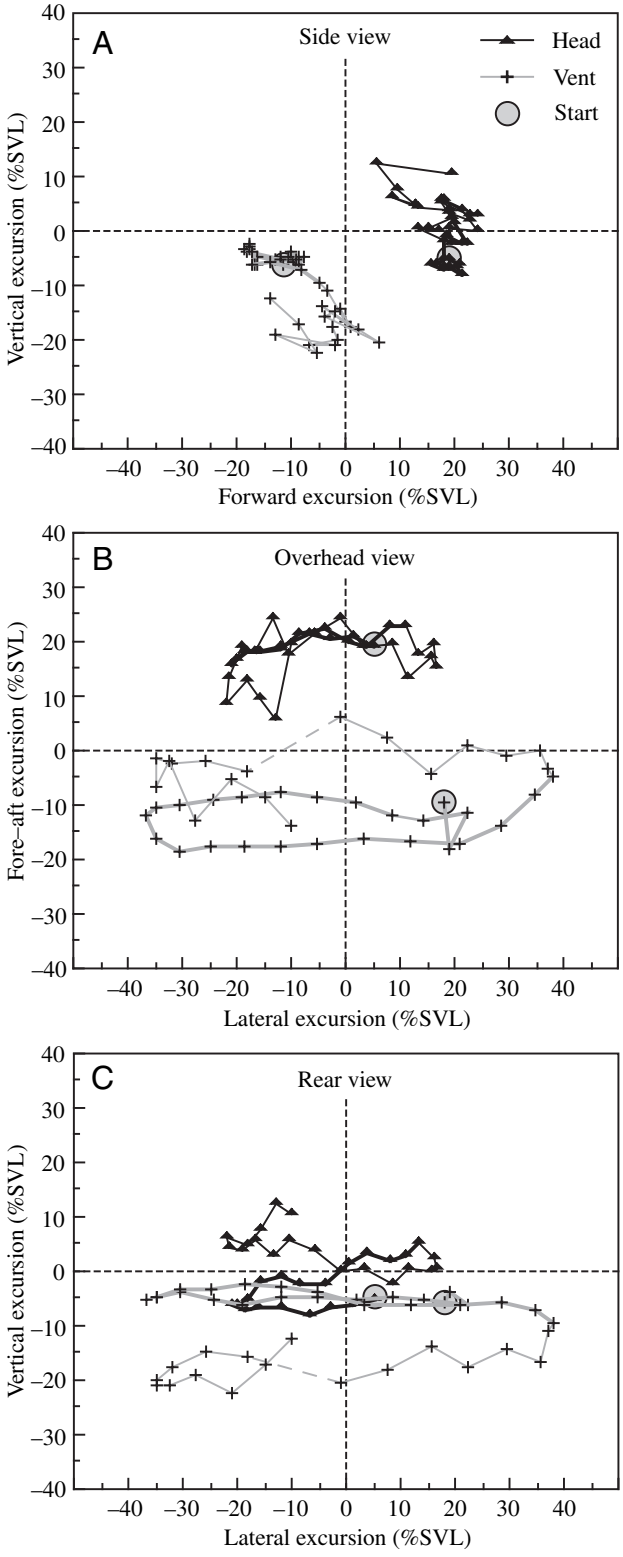

Fig. 10. Side view (A), overhead view (B) and rear view (C) of excursion during the shallowing phase in one trajectory. The midpoint is at the center of each figure. The beginning of the sequence is indicated with gray circles. The first undulatory cycle is represented by thick lines. Missing data are represented by dashes. For most of the sequence, the head is roughly vertically aligned and about 20% SVL forward of the midpoint. The vent begins slightly lower than midpoint and is moved downward and forward in the second undulatory cycle. The head and vent move side-to-side in phase, with the head using a smaller amplitude than the vent. (M=26 g, SVL=62 cm.)

These interpretations are clouded by the variance in the speed data, which exhibit oscillations of varying period and amplitude (e.g. Figs 6 and 8). These oscillations may be real, perhaps the result of the midpoint of the snake not coinciding with the effective center of gravity; as the snake undulates and changes orientation, the lift-to-drag ratio may be constantly changing, which would constantly change both speed and glide angle. Unfortunately, errors in the coordinate data were too high to identify and correlate such fine-scale changes in posture, speed and glide angle. Observed oscillations in speed may also be due to systematic error – as the snake moved away from the cameras, the coordinate position error increased. Furthermore, identifying the center of gravity as posture changes requires data on the tail's position, which were not collected here; although the tail is thin, it may have a significant effect on center of gravity due to its length (~30% SVL). Trends in speed should be easier to identify in the future using longer glide sequences and improved photogrammetric resolution.

In a comprehensive study of gliding lizards (*Draco* spp.), McGuire (1998) observed a stabilization of airspeed in some trials, but did not observe glides in which the rate of increase of airspeed simply declined after a transition. In some trials, the airspeed of the lizard increased and then decreased with no equilibrium period, which he termed a 'velocity peak'. In most of these velocity peak glides, the lizard landed on a pole; he therefore interpreted the decrease in airspeed as a preparation for landing. He also observed a concomitant upswing in the trajectory before landing, so it is likely that the lizard was stalling in preparation for landing. Flying squirrels are known to perform a similar stalling behavior by radically increasing the angle of attack, which slows the squirrel down and pitches

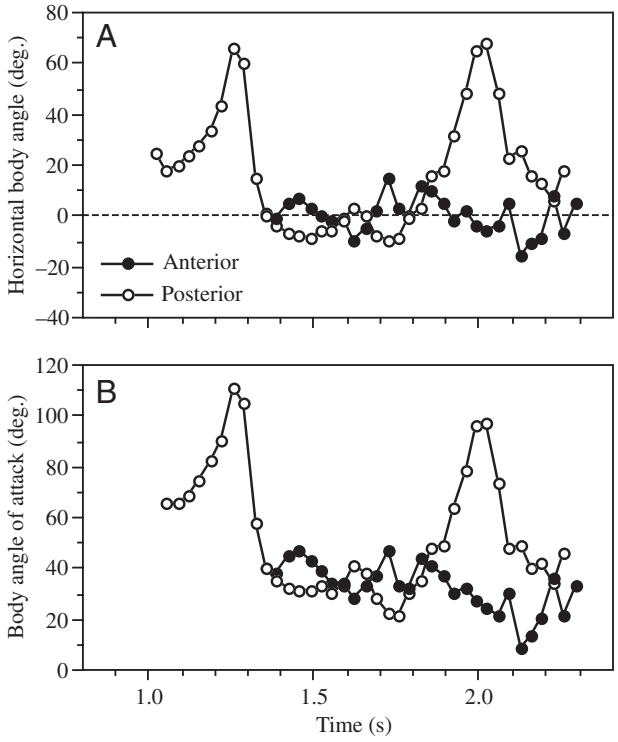

Fig. 11. Horizontal body angle (*HBA*) and body angle of attack *vs* time in the shallowing glide phase of one trajectory. The videocameras were stationed lower on the tower to record the end of the trajectory only; as such an arbitrary time was assigned to the beginning of the sequence. A. Anterior HBA (filled circles) was relatively constant around 0°, meaning that the anterior body was oriented approximately parallel with the ground. The posterior HBA (unfilled circles) cycled to greater than 60°, indicating that the posterior body swung below the horizontal. B. The pattern of body angle of attack is similar to that of HBA. However, because the glide angle was decreasing throughout this sequence, both anterior and posterior body angles of attack declined relative to HBA. Only the anterior body angle of attack, which changed from about 40° to 20° during the sequence, is a good proxy for true angle of attack. (M=16 g, SVL=54 cm.)

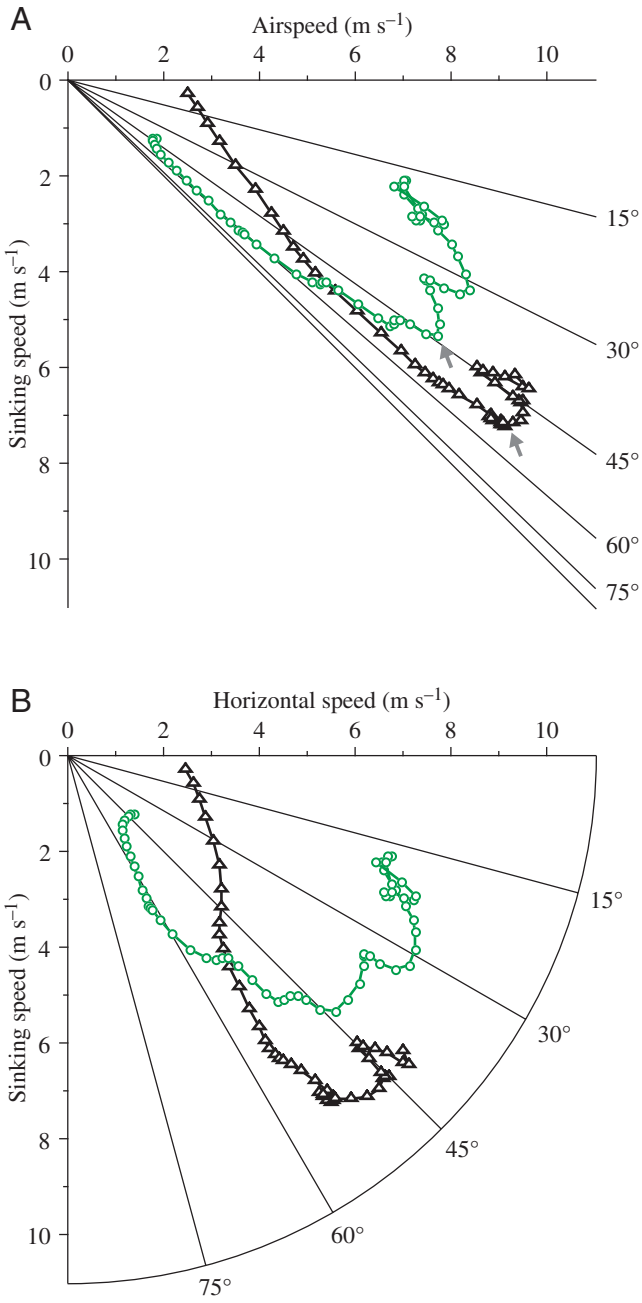

Fig. 12. Performance and velocity polar diagrams (following Tucker, 1998) for two trajectories, representing a small snake (circles; M=11 g, SVL=47 cm) and a large snake (triangles; M=83 g, SVL=85 cm). The straight lines indicate speed combinations resulting in constant glide angle. (A) Performance diagram. The larger snake had a higher initial airspeed and greater rate of sinking speed increase. Sinking speed increased in linear fashion until reaching transition, which occurred at a higher airspeed for the larger snake (arrow). (B) Velocity polar diagram.

the body upward, enabling an upright landing on a vertical substrate (Nachtigall, 1979; Scholey, 1986; Stafford et al., 2002). None of the snakes in this study landed on a vertical substrate, but they were not observed to slow down before landing on the ground.

Glide equilibrium

When discussing a glider's aerodynamic characteristics, it is important to describe its performance during equilibrium. A glider can use a range of equilibrium speed and glide angle combinations (usually plotted in a 'glide polar'; see Fig. 12). This range defines the limits of its gliding ability. If in equilibrium at its minimum speed, the glider maximizes its time aloft; at its minimum glide angle, it maximizes its distance traveled. By definition, force equilibrium assumes that the forces are balanced on the glider and that there is no net acceleration. There was no unequivocal evidence for force equilibrium on the snakes given the combination of changing airspeed, sinking speed and horizontal speed in most analyzed trials. It is therefore unclear what factors contribute to how quickly the snakes may attain equilibrium. It is also unclear whether or not the snakes even attempted to reach equilibrium

– if they purposefully chose landing locations closer than their ability limits, equilibrium gliding may not have been necessary. Regardless, it is theoretically possible for *C. paradisi* to attain equilibrium if launched from a sufficient vertical height. Indeed, unobstructed space for aerial locomotion is ample in the mixed dipterocarp forests it inhabits; canopy stratification is pronounced and emergent trees of prominent heights are frequent (Dudley and DeVries, 1990; Richards, 1996; Whitmore, 1992). Considering that some snakes may have reached equilibrium in this study when jumping from a height of 9.6 m, it is possible that snakes attain equilibrium gliding when taking off from greater heights in the wild, given sufficient horizontal space. Conversely, equilibrium gliding may be precluded due to insufficient space between trees, or because fully developed snake flight may be inherently unsteady, independent of starting height.

One trial showed evidence of equilibrium, with a short region where all three speeds were approximately constant (Fig. 6) before the snake traveled out of view of the cameras. This snake, which consistently gave long glide sequences, was the second smallest of the sample. It also gave the farthest glide on record – in an exceptional glide, the snake traveled a horizontal distance of 21 meters, 30% farther than any of the other 237 trials. Because only the first 1.2 s (~22%) of this trajectory was recorded by videocameras (and therefore was not included as one of the 14 'full' trajectories described herein), the unknown portion of the trajectory could be not be determined. However, the lowest measured glide angle for recorded trajectories was 13°, which suggests that the glide angle in the exceptional trajectory reached magnitudes equal to or lower than 13°. Furthermore, because this glide was much longer than all others, it seems the likeliest to have contained an equilibrium component.

By comparison, McGuire (1998) found a large percentage (48% of 150) of his flying lizard glide trials to have an equilibrium component. Because the lizards were launched from a lower starting point (6 *vs* 9.6 m), they must have used shorter ballistic dives and/or higher shallowing rates than did the snakes. Generally lizards with lower wing loadings reached equilibrium more often, but the largest lizards (with wing loadings of about 25 N m^{-2}) reached it too.

Given that equilibrium did not conclusively occur in the trials analyzed here, the average minimum glide angle reported for *C. paradisi*, 28°, is a conservative estimate. The range of minimum glide angles was 13–46°, with smaller gliders attaining lower glide angles than larger snakes. However, it is possible that these snakes are capable of reaching the same minimum glide angle given a great enough starting height. If true, then ballistic dive distance, trajectory shallowing rate, or horizontal distance traveled may be better indices of performance than minimum glide angle for *C. paradisi*.

Aerodynamic characteristics

To estimate the range of aerodynamic characteristics in *C. paradisi*, we calculated basic aerodynamic parameters using performance values from two representative snakes, one small and one large (M=11 and 63 g, SVL=47 and 83 cm). The small snake was the best glider of any snake observed. The calculations below use data from a phase late in the trajectories where the airspeed had stabilized or was approaching stability.

To estimate the snake's average lift coefficient late in the trajectory, we assume that all forces acting on the snake are in equilibrium and that the airfoil is parallel with the ground. L and D are the lift and drag forces, which act perpendicular and parallel to the glide path, respectively; R is the resultant aerodynamic force, which acts upward; W is the weight of the snake; and α is the angle of attack. An equation for lift coefficient at high Reynolds numbers (Vogel, 1994) is:

$$C_L = \frac{2L}{\rho S U^2}, \quad (5)$$

where C_L is the lift coefficient, ρ is the density of air at 30°C (the field temperature), S is the projected surface area in plan view and U is the airspeed. The lift force is equal to the resultant aerodynamic force, R, multiplied by the cosine of the glide angle,

$$L = R\cos\gamma . \quad (6)$$

Because the forces are in equilibrium, the total aerodynamic force is equal to the weight of the snake,

$$L = W\cos\gamma . \quad (7)$$

Substituting this expression for lift and wing loading (WL) for the weight divided by the projected surface area in equation 5 yields the following:

$$C_L = \frac{2WL\cos\gamma}{\rho U^2} . \quad (8)$$

Using an air density value of 1.165 kg m^{-3} (at 30°C), airspeeds of 7 and 10 m s^{-1} for the small and large snakes, respectively, and wing loadings of 18 and 31 N m^{-2}, the average calculated lift coefficients are 0.63 and 0.53. Actual instantaneous lift coefficients during the glide may vary substantially.

The Reynolds number (Re) can be calculated following Vogel (1994). Here we assume that the flattened width of the snake (approximately twice the resting width; Socha, 2002b) is the characteristic length. Using a kinematic viscosity of 15.94×10^{-6} m^2 s^{-1} at 30°C and flattened widths of 1.2 and 2.4 cm for the small and large snakes, respectively, the approximate Reynolds numbers are 5000 and 15,000.

Aspect ratio is calculated using the span and area of a flyer's wings. However, it is not immediately obvious which parts of the snake act as a functional 'wing' from which to measure span. If the span is considered to be the maximum length of snake between curves, the aspect ratios of the small and large snake are about 13 and 11, respectively. If it is assumed that only the relatively straight sections of body between the curves as the 'wing', the aspect ratios are about 10 and 8, respectively. In either case, the 'aspect ratio' of *C. paradisi* is high relative to most other vertebrate gliders.

The maximum lift-to-drag ratios can be estimated using the

minimum glide angle. With minimum observed glide angles of 20° and 40° for the small and large snake, respectively, the lift-to-drag ratios are 2.7 and 1.2. In the trial with the lowest recorded glide angle (13°), the calculated lift-to-drag ratio is 4.3.

Postural influences on snake flight

Although no precise association of changes in posture with changes in glide angle were observed here, these data suggest four hypotheses for behavioral influences on lift generation. (1) In the S-formation phase, more of the snake's body becomes perpendicular to the airflow as the snake pulls itself into the 'S' posture. In effect, the body changes from a spear to a biplane. This orientation drastically increases the snake's aspect ratio and therefore should generate more lift than a mostly straight snake. (2) As the snake pitches downward, the chords of the snake's 'airfoils' rotate into a position more favorably aligned with the oncoming airflow, suggesting that the snake becomes less like a bluff body (in which drag dominates) and more like an airfoil (in which lift dominates). (3) The shallowing glide, in which the glide angle decreases, begins only after the snake is fully undulating, suggesting that aerial undulation itself may increase the lift-to-drag ratio. (4) Alternatively, changes in glide angle are solely a result of increasing speed due to gravity, suggesting that behavior has no effect on lift generation. Considering the abrupt transitions in speed, this scenario seems unlikely. A combination of physical modeling, live-animal manipulation (for example, attaching weights to the body to alter mass distribution in flight) and statistical analyses of performance (e.g. Socha and LaBarbera, 2005) are required to fully explore these behavioral hypotheses.

Aerial undulation is one of the most striking features of flying snake locomotion. No other glider makes such pronounced undulatory motions with its body while gliding, and its function during flight is uncertain. Given that lateral undulation is the dominant mode of locomotion in snakes (Pough et al., 2001), aerial undulation may simply be a behavioral vestige with no function. Some non-flying snakes, in fact, undulate when dropped from a height (J.J.S., unpublished). However, given its prominent role in gliding flight, it seems unlikely that aerial undulation has no aerodynamic function. The side-to-side movement adds an additional component of speed over the body in addition to the airspeed; however, this component is so small that the additional lift it would produce is marginal. Other possible functions include dynamic stabilization, in which the changing posture would serve to move the centers of gravity and pressure in a way that allows controllable flight. In a study that explicitly addressed the effects of behavior on performance (Socha and LaBarbera, 2005), undulation amplitude was found to have a far greater influence than undulation frequency. Future modeling studies will detail how specific aspects of undulation amplitude and frequency relate to aerodynamic force production or stabilization.

Aerial undulation is kinematically different from lateral undulation on the ground, in which constant points of contact are maintained, or in water, in which traveling waves increase in magnitude along the body. In a pilot study, Socha (1998) recorded the aerial, terrestrial and aquatic locomotion of four *C. paradisi* specimens. For both water and land, the forward speed of the snake was much lower (1.0–1.5 m s^{-1}), the undulation frequency was almost three times higher (3–4 Hz) and the wave height was smaller (~7–14% SVL) than in air. The shape of the waves was also different – during terrestrial locomotion, the waves were similar in size along the snake, and in swimming, the size of the waves increased as they traveled down the body. Although both are consistent with normal snake locomotion, neither undulation pattern resembles the high-amplitude 'S' shape used in aerial undulation.

Comparative performance

Considering the snake's unorthodox locomotor style, it is relevant to ask how snake aerial locomotion compares to that of other vertebrate gliders. However, it is first important to note the differences in methods employed in other gliding studies. Generally, animal gliders have been observed moving through the air in their natural habitats. In these field studies (e.g. Ando and Shiraishi, 1993; Jackson, 1999; Scholey, 1986; Stafford et al., 2002; Vernes, 2001), glide performance was estimated using a few basic measurements, such as takeoff height, landing height and horizontal distance (all usually estimated using a rangefinder or maps); and aerial time (measured with a stopwatch). Because straight-line distances were used to calculate performance in these studies, true glide ratio (valid only at equilibrium) and speed are underestimated – the animals actually achieved higher glide ratios and higher speeds during the gliding portion of the trajectory than reported. For some gliders, performance metrics have only been reported from anecdotal observations, with distances estimated by eye (e.g. *Hyla milaria*, as described in Duellman, 1970). Whereas some observers make credible judgments of distance, others seem implausible (e.g. glide ratios of 11–13 for colugos, Lekagul and McNeeley, 1977; and a gliding distance of 450 m for a flying squirrel, Nowak, 1999). In other studies, accuracy cannot be evaluated because glide performance is cited without mentioning methods (e.g. Kawachi et al., 1993). These studies are important in establishing an estimate of performance and placing gliding in an ecological context, but do not address kinematic details. By contrast, McGuire's (1998) study of 11 species of flying lizards (*Draco*), in which he digitized the lateral view of 150 trajectories at 12 Hz to calculate instantaneous glide angles, had a much higher temporal and spatial resolution than previous studies. However, because his reported glide ratio values were calculated based on the takeoff and landing points only, peak performance was also underestimated.

The shape of *C. paradisi*'s trajectory appears to be similar to that of other gliders, with a steep initial dive followed by a shallowing glide. Snakes lost 1–5 m of vertical height at a glide angle of 52–62° during the ballistic dive. In comparison, Scholey (1986) estimated that the giant red flying squirrel,

Petaurista petaurista (mass ~1.3 kg), traveled through the ballistic dive at a glide angle of 50–70° while losing 6 m of vertical height, and Vernes (2001) used a regression of horizontal distance *vs* vertical distance traveled to estimate a ballistic dive of 1.9 m in the northern flying squirrel, *Glaucomys sabrinus* (mass ~93 g). However, these comparisons should be viewed with caution because it is unclear to what extent the inferentially estimated ballistic dive estimates correspond to the quantitatively measured ballistic dives in this study.

When considering glide angle, *C. paradisi* are better gliders than 'parachuting' lizards (*Ptychozoon* sp.; Marcellini and Keefer, 1976; Young et al., 2002), on a par with some gliding mammals (e.g. *Petaurus breviceps* and *Petaurista leucogenys*; Nachtigall, 1979; Ando and Shiraishi, 1993) and poorer gliders than some gliding lizards (*Draco* spp.; McGuire, 1998) and flying fish (e.g. *Cypselurus* spp.; Davenport, 1992). As in these other flyers, *C. paradisi* is potentially capable of using aerial locomotion to move effectively between trees, chase aerial prey, or avoid predators. Airspeed and wing loading also fall within the range of other gliders (Rayner, 1981).

There have been fewer accurate reports of body orientation during gliding. Flying squirrels and flying lizards orient their bodies approximately parallel with the horizontal plane while gliding (McGuire, 1998; Nachtigall, 1979; Scholey, 1986), such that the angle of attack is approximately the same as the glide angle. This also seems to be true of *C. paradisi* when considering the anterior segment alone. For these gliders, this parallel body orientation may be a compromise between choosing an angle of attack that maximizes the lift-to-drag ratio and keeping the landing location and nearby obstacles within the field of view.

Chrysopelea and *Draco*, to our knowledge, are the only predator/prey system in which both taxa glide. It has been suggested (R. Dudley, personal communication) that their respective gliding abilities may have been subject to an evolutionary arms race. This hypothesis is plausible considering their respective gliding performance ability. *Draco* is the better glider in some respects, with a higher lift-to-drag ratio, shorter ballistic dive and likely higher maneuverability, but its range of performance within the genus overlaps that of *C. paradisi*, and *C. paradisi* may glide faster. Faster gliding is better for linear pursuit, but once the *Draco* turns, its lower speed and lower wing loading would make it difficult to intercept. Furthermore, *Chrysopelea* actively hunt their prey, likely have good vision for a snake (see Socha and Sidor, in press) and as lizard eaters (Flower, 1899) are reported to take *Draco* in their diet (Wall, 1908). Historically, it cannot be determined if their gliding abilities co-evolved, but it is possible in principal to observe whether *Chrysopelea* chases *Draco* in the wild.

Conclusions

C. paradisi are true gliders. Their style of gliding flight, in which a cylindrical animal becomes flattened, coils into an 'S' shape and aerially undulates, has no analogue in the natural or engineering world. Its aerial undulation involves complex kinematics in which the body moves in and out of the horizontal plane, for which the aerodynamic consequences are unknown. Although the results presented here unequivocally show that *C. paradisi* does produce significant horizontal motion in flight, it is still unclear which aspects of behavior and morphology are responsible for the generation of aerodynamic forces. Such forces allow the snake to gain horizontal distance and to turn, all accomplished without tumbling over and using no obvious morphological control surfaces. To address these aerodynamic issues, we have begun to investigate snake flight using physical models to isolate specific effects of shape, and plan to conduct parallel computational modeling studies that examine the effects of the snake's complex kinematics.

We thank the Zoological Gardens of Singapore staff for support, in particular W. H. Cheng, S. Chandran, S. Herbert, F. Lim and P. Martelli. T. Chong, C. C. Kong, D. Lau, D. Lauw, K. Lim, N. Lim, W. Lim, Y. Lin, K. Su, K. Y. Tan, S. K. Tng, W. Toh, J. Wong, Y. Yatiman, T. K. Yen, J. Yeo, L. YeQiang and F. Yuwono provided help with snake handling and equipment operation. We thank K. Lim, N. Sivasothi, T. H. Hui, S. Rashid and members of the P. Ng lab for logistical support. We thank R. Dudley, M. LaBarbera, J. McGuire, H. Voris, M. Westneat and the University of Chicago Biomechanics Group for discussion and advice. C. Abraczinskas provided generous illustration advice. P. Magwene provided the instantaneous glide angle calculation methodology. C. Diteresi provided help with digitization. We appreciate M. LaBarbera, R. Dudley, M. Hale, G. Byrnes, K. Bishop and two anonymous reviewers for comments and critical reading of the manuscript. This work was supported by grants from the National Geographic Society, the Journal of Experimental Biology, the Explorers Club, Sigma Xi, the Hinds Fund and the Chicago Herpetological Society.

List of symbols

D	drag force
L	lift force
R	total aerodynamic force
C_L	coefficient of lift
HBA_n	horizontal body angle
m	mass
Re	Reynolds number
S	projected area
SVL	snout–vent length
U	airspeed
W	weight (mg)
WL	wing loading
x, y	image coordinates
X, Y, Z	spatial coordinates
$\alpha_{B,n}$	body angle of attack
γ_{BD}	ballistic dive angle
γ_n	instantaneous glide angle
ρ	density of air

References

Abdel-Aziz, Y. I. and Karara, H. M. (1971). Direct linear transformation from comparator coordinates into object space coordinates in close-range photogrammetry. In *Proc. ASP/UI Symp. Close-Range Photogrammetry*, pp. 1-18. Falls Church, VA: American Society of Photogrammetry.

Ambrosio, J., Abrantes, J. and Lopes, G. (2001). Spatial reconstruction of human motion by means of a single camera and a biomechanical model. *Hum. Mov. Sci.* **20**, 829-851.

Ando, M. and Shiraishi, S. (1993). Gliding flight in the Japanese giant flying squirrel *Petaurista leucogenys*. *J. Mamm. Soc. Japan* **18**, 19-32.

Bertin, J. J. (2001). *Aerodynamics for Engineers*. Upper Saddle River, NJ: Prentice Hall College Division.

Caple, G., Balda, R. P. and Willis, W. R. (1983). The physics of leaping animals and the evolution of preflight. *Am. Nat.* **121**, 455-476.

Chen, L., Armstrong, C. W. and Raftopoulos, D. D. (1994). An investigation on the accuracy of 3-dimensional space reconstruction using the direct linear transformation technique. *J. Biomech.* **27**, 493-500.

Daly, M. (1899). A flying snake. *J. Bombay Nat. His. Soc.* **XII**, 589.

Davenport, J. (1992). Wing-loading, stability and morphometric relationships in flying fish (Exocoetidae) from the north-eastern Atlantic. *J. Mar. Biol. Ass. UK* **72**, 25-39.

de Groot, J. H., van der Sluijs, I., Snelderwaard, P. C. and van Leeuwen, J. L. (2004). A 3-D kinematic analysis of tongue flicking in Python molurus. *J. Exp. Biol.* **207**, 827-839.

Dial, R. (2003). Energetic savings and the body size distributions of gliding mammals. *Evol. Ecol. Res.* **5**, 1-12.

Dudley, R. and DeVries, P. (1990). Tropical rain forest structure and geographical distribution of gliding vertebrates. *Biotropica* **22**, 432-434.

Duellman, W. E. (1970). The hylid frogs of Middle America. *Monograph of the Museum of Natural History, the University of Kansas* **1**.

Emerson, S. B. and Koehl, M. A. R. (1990). The interaction of behavioral and morphological change in the evolution of a novel locomotor type: 'flying' frogs. *Evolution* **44**, 1931-1946.

Flower, S. S. (1899). Notes on a second collection of reptiles made in the Malay Peninsula and Siam, from November 1896 to September 1898, with a list of the species recorded from those countries. *Proc. Zool. Soc. Lond.* **May 16**, 682-685.

Gruen, A. (1997). Fundamentals of videogrammetry – A review. *Hum. Mov. Sci.* **16**, 155-187.

Heyer, W. R. and Pongsapipatana, S. (1970). Gliding speeds of *Ptychozoon lionatum* (Reptilia: Gekkonidae) and *Chrysopelea ornata* (Reptilia: Colubridae). *Herpetologica* **26**, 317-319.

Jackson, S. M. (1999). Glide angle in the genus *Petaurus* and a review of gliding in mammals. *Mamm. Rev.* **30**, 9-30.

Kawachi, K., Yoshinobu, I. and Azuma, A. (1993). Optimal flight path of flying fish. *J. Theor. Biol.* **163**, 145-159.

Lekagul, B. and McNeeley, J. A. (1977). *Mammals of Thailand*. Bangkok: Sahakarnbhat.

Maas, H.-G. (1997). Concepts of real-time photogrammetry. *Hum. Mov. Sci.* **16**, 189-199.

Marcellini, D. L. and Keefer, T. E. (1976). Analysis of the gliding behavior of *Ptychozoon lionatum* (Reptilia: Gekkonidae). *Herpetologica* **32**, 362-366.

McCay, M. G. (2001). Aerodynamic stability and maneuverability of the gliding frog *Polypedates dennysi*. *J. Exp. Biol.* **204**, 2817-2826.

McGuire, J. (1998). Phylogenetic systematics, scaling relationships and the evolution of gliding performance in flying lizards (Genus *Draco*). PhD Thesis. University of Texas, Austin, TX, USA.

Meintjes, E. M., Douglas, T. S., Martinez, F., Vaughan, C. L., Adams, L. P., Stekhoven, A. and Viljoen, D. (2002). A stereo-photogrammetric method to measure the facial dysmorphology of children in the diagnosis of fetal alcohol syndrome. *Med. Eng. Physics* **24**, 683-689.

Mertens, R. (1968). Die Arten und Unterarten der Schmuckbaumschlangen (*Chrysopelea*). *Senckenbergiana biologica* **49**, 191-217.

Mertens, R. (1970). Zur Frage der 'Fluganpassungen' von *Chrysopelea* (Serpentes, Colubridae). *Salamandra* **6**, 11-14.

Mundkur, T. (1978). A note on reproduction in the flying snake *Chrysopelea ornata* (Shaw). *J. Bombay Nat. Hist. Soc.* **75**, 854-859.

Nachtigall, W. (1979). Gleitflug des flugbeutlers *Petaurus breviceps papuanus* (Thomas) II. *J. Comp. Physiol.* **133**, 89-95.

Norberg, R. A. (1981). Why foraging birds in trees should climb and hop upwards rather than downwards. *Ibis* **123**, 281-288.

Norberg, R. A. (1983). Optimal locomotion modes of foraging birds in trees. *Ibis* **125**, 172-180.

Norberg, U. M. (1985). Evolution of vertebrate flight: an aerodynamic model for the transition from gliding to active flight. *Am. Nat.* **126**, 303-327.

Norberg, U. M. (1990). Vertebrate Flight. Berlin: Springer-Verlag.

Norberg, U. M., Brooke, A. P. and Trewhella, W. J. (2000). Soaring and non-soaring bats of the family Pteropodidae (Flying foxes, *Pteropus* spp.): wing morphology and flight performance. *J. Exp. Biol.* **203**, 651-664.

Nowak, R. M. (1999). *Walker's Mammals of the World*. Baltimore, MD: Johns Hopkins University Press.

Oliver, J. A. (1951). 'Gliding' in amphibians and reptiles, with a remark on an arboreal adaptation in the lizard, *Anolis carolinensis carolinensis* Voigt. *Am. Nat.* **85**, 171-176.

Pendlebury, H. M. (1931). A 'flying' snake. *Bull. Raffles Museum* **5**, 75.

Pough, H., Cadle, J., Crump, M., Savitzky, A. and Wells, K. (2001). *Herpetology*. Upper Saddle River, NJ: Prentice Hall.

Rayner, J. M. V. (1981). Flight adaptations in vertebrates. *Symp. Zool. Soc. Lond.* **48**, 137-172.

Richards, P. W. (1996). *The Tropical Rain Forest: An Ecological Study.* Cambridge: Cambridge University Press.

Scheibe, J. S. and Robins, J. H. (1998). Morphological and performance attributes of gliding mammals. In *Ecology and Evolutionary Biology of Tree Squirrels*, vol. 6 (ed. J. F. Merritt and D. A. Zegers), pp. 131-144. Martinsville, VA: Virginia Museum of Natural History.

Scholey, K. D. (1986). The climbing and gliding locomotion of the giant red flying squirrel *Petaurista petaurista* (Sciuridae). In *Biona Report 5, Bat flight – Fledermausflug*, W. Nachtigall (ed. W. Nachtigall), pp. 187-204. Stutgart: Gustav Fischer.

Shelford, M. A. (1906). A note on 'flying' snakes. *Proc. Zool. Soc. Lond.* **1**, 227-230.

Socha, J. J. (1998). A description of 'flight' kinematics in the flying snake, *Chrysopelea paradisi*. *Am. Zool.* **38**, 150A.

Socha, J. J. (2002a). The biomechanics of flight in snakes. PhD Thesis. University of Chicago, IL, USA.

Socha, J. J. (2002b). Gliding flight in the paradise tree snake. *Nature* **418**, 603-604.

Socha, J. J. and LaBarbera, M. (2005). Effects of size and behavior on aerial performance of two species of flying snakes (*Chrysopelea*). *J. Exp. Biol.* **208**, 1835-1847.

Socha, J. J. and Sidor, C. A. (in press). *Chrysopelea* spp. (Flying Snakes). Behavior. *Herpetol. Rev.*

Stafford, B. J., Thorington, R. W. and Kawamichi, T. (2002). Gliding behavior of Japanese giant flying squirrels (*Petaurista leucogenys*). *J. Mammalogy* **83**, 553-562.

Tucker, V. (1998). Gliding flight: speed and acceleration of ideal falcons during diving and pull-out. *J. Exp. Biol.* **201**, 403-414.

Tweedie, M. W. F. (1960). The Malayan gliding reptiles. *Proc. South London Entomol. and Nat. Hist. Soc.* **1959**, 97-103.

Tweedie, M. W. F. (1983). *The Snakes of Malaya.* Singapore: Singapore National Printers.

Vaughan, C. L., Douglas, T. S. V. and Wynne, S. M. (2004). 3-D point localisation in low-dose X-ray images using stereo-photogrammetry. *Med. Biol. Eng. Comp.* **42**, 37-43.

Vaughn-Arbuckle, K. H. (1959). Flying snakes. *J. Bombay Nat. His. Soc.* **56**, 640-642.

Vernes, K. (2001). Gliding performance of the northern flying squirrel (*Glaucomys sabrinus*) in mature mixed forest of Eastern Canada. *J. Mammalogy* **82**, 1026-1033.

Vogel, S. (1994). *Life in Moving Fluids*. Princeton: Princeton University Press.

Walker, J. A. (1997). QuickSAND. Quick Smoothing and Numerical Differentiation for the Power Macintosh.

Walker, J. A. (1998). Estimating velocities and accelerations of animal locomotion: a simulation experiment comparing numerical differentiation algorithms. *J. Exp. Biol.* **201**, 981-995.

Wall, F. (1908). A popular treatise on the common Indian snakes, Part 6. *J. Bombay Nat. His. Soc.* **18**, 227-243.

Whitmore, T. C. (1992). *An Introduction to Tropical Rain Forests*. Oxford: Oxford University Press.

Young, B. A., Lee, C. E. and Daley, K. M. (2002). On a flap and a foot: aerial locomotion in the 'flying' gecko, *Pychozoon kuhli*. *J. Herpetol.* **36**, 412-418.

Yuan, X. H. and Ryd, L. (2000). Accuracy analysis for RSA: a computer simulation study on 3D marker reconstruction. *J. Biomech.* **33**, 493-498.